MINERALOGICAL MAGAZINE, SEPTEMBER 1985, VOL. 49, PP. 495–504

The distribution of the rare earth elements within the Carnmenellis Pluton, Cornwall

N. L. JEFFERIES*

Department of Geology, The University, North Park Road, Exeter, Devon

ABSTRACT. The Carnmenellis pluton is a post-orogenic granite of Hercynian age, comprised largely of porphyritic biotite granites which possess *LREE* enriched patterns with slight negative Eu anomalies. Electron microprobe and ICP spectrometry data are presented for monazite, which occurs as an accessory mineral in all granite types, and it is demonstrated that this mineral is the principal host for *LREE* in the biotite granites. *HREE* are strongly partitioned into the accessory minerals xenotime, apatite, and zircon; only Eu substitutes significantly into the essential minerals. The behaviour of the *REE* during granite differentiation is controlled by the behaviour of the radioactive accessory minerals, which limits the usefulness of these elements in the petrogenetic modelling of granitic rocks.

KEYWORDS: rare earth elements, granite, monazite, Carnmenellis pluton, Cornwall.

TRACE ELEMENT modelling with the rare earth elements has been widely used in petrogenetic studies of granitic rocks (Compton, 1978; Hanson, 1978). It is generally recognized that a proportion of the *REE* do not substitute in trace amounts into essential minerals, as is the case with basic igneous rocks, but instead are concentrated within the accessory mineral assemblages (McCarthy and Kable, 1978; Fourcade and Allegre, 1981). Pagel (1982) showed that the concentration of *REE* within minerals such as zircon, allanite, and monazite complicates the interpretation of *REE* data from granitic rocks owing to the variable crystallization behaviour and zonation of these minerals.

Many studies of the radioactive accessory minerals of European U-rich granites of Hercynian age have been made (Le and Stussi, 1973; Basham *et al.*, 1982) and the various parageneses identified. As a result these granites have been subdivided into two categories which could be distinguished by their accessory minerals (Pagel, 1982). The subdivisions are (1) subalkaline potassic granites which are characterized by the assemblage apatite–zircon–thorite–sphene–allanite and rare ThO_2-rich uraninite, and (2) leucocratic granites, which contain the accessory mineral assemblage monazite–zircon–apatite–xenotime–ThO_2-poor-uraninite and Ti oxides. The biotite granites of SW England fall into the second category (Basham *et al.*, 1982; Jefferies, 1984). This paper examines the influence of the accessory mineral assemblage upon *REE* patterns within one of the plutons of this batholith.

* Present address: Chemical Technology Division, Building 10.5, AERE, Harwell, Oxfordshire.

The Carnmenellis pluton

The Hercynian batholith of SW England is exposed as a series of post-orogenic, discordant plutons which extend, in a linear trend, from Dartmoor to the Scilly Isles. The Carnmenellis pluton was originally mapped in detail by Ghosh (1934) and is largely composed of porphyritic biotite granites into which two bosses of fine-grained granite have been intruded. The biotite granites are cut by microgranite sheets, typically less than 50 cm in width, which have been emplaced into fracture planes within the pluton.

Ghosh (1934) identified three phases of porphyritic biotite granites which he labelled Types I, II, and III (fig. 1). Type III granite is a medium-grained porphyritic biotite granite which occupies the central part of the pluton. This is considered to be intrusive into the coarse-grained porphyritic biotite granites which surround it. Ghosh distinguished two phases of coarse-grained granite in the field on textural criteria (Types I and II) but more recent authors (Chayes, 1955; Al Turki and Stone, 1978) conclude that they are modally and chemically identical, and should not be regarded as separate units. However, the nomenclature of Ghosh (1934) will be used in this paper as it is based upon regional mapping of the pluton.

Petrology of the biotite granites

All the porphyritic biotite granites possess identical mineralogy and display similar microscopic features and so are considered as a single

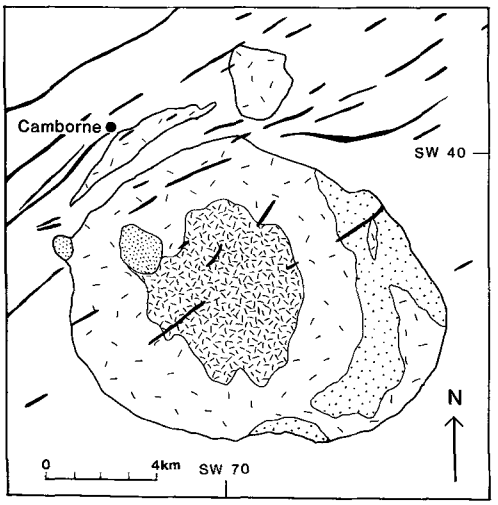

FIG. 1. Locality map of the Carnmenellis pluton.

group. Modal data for the biotite granites are presented by Al Turki and Stone (1978); all are two-mica granites, although from textural studies muscovite is considered to have a subsolidus origin (Stone, 1979).

Jefferies (1984) studied the radioactive accessory mineral assemblage of the porphyritic biotite granites which consisted of monazite-zircon-apatite-xenotime and ThO_2-poor-uraninite. Radioactive accessory minerals, located using the technique of α-autoradiography, were examined using an energy dispersive Link microanalyser attached to a Phillips 501B Scanning Electron Microscope. The Link microanalyser was used in a qualitative mode to identify monazite, xenotime, zircon, and uraninite. In this study of 1200 radioactive minerals from Type I granite it was found that monazite comprised 48%, zircon 48%, uraninite 3%, and xenotime 1% of the radioactive accessory minerals examined.

Textural evidence suggests that these accessory minerals crystallized at an early magmatic stage, as they are commonly associated with clusters of apatite and ilmenite which occur as inclusions in all major minerals. The remaining radioactive accessory minerals occur as individual crystals within biotite, the feldspars and quartz.

Electron microprobe analyses

Chemical analyses of monazites from Type I granite were obtained using the wavelength dispersive Microscan 9 electron microprobe at the Geology Department, University of Oxford. The analyses are given in Table I. Formulae are calculated on the basis of 16 oxygens. The stoichiometry obtained from these analyses is in good agreement with those presented by Deer *et al.* (1962) where, ideally, $P+Si = 4.00$ cations per formula unit. In this study $P+Si$ ranges from 3.89–3.98.

Gramaccioli and Segalstad (1978) discussed the possible substitutions which allow U^{4+} and Th^{4+} to enter into monazite. The substitution of tetravalent U and Th into the trivalent *REE* position must be balanced by the presence of ions of lower charge substituting into the tetrahedral or octahedral positions. Three substitutions were recognized: $Si^{4+} \rightleftharpoons P^{5+}$, $Ca^{2+} \rightleftharpoons REE^{3+}$, and $K^{+} \rightleftharpoons REE^{3+}$.

Three electron microprobe traverses of monazite crystals are given in fig. 2. All elements are calculated as atomic proportions: analytical precision is approximately ±5%, and error bars are therefore added in fig. 2. No zonation of the monazite crystals is visible optically, and only a weak chemical zonation is discernible from the microprobe analyses. Th, Ca, and Ce zonation within the crystals is not detected; Sm and Y show slight increases from the core to the rim in two out of the three traverses each, whilst Dy is only present in amounts above the lower limit of detection in the rims of two of the crystals.

Since the chemical zonation within individual crystals is weak, the atomic substitutions within monazite are best shown using two element variation diagrams, the elements again being calculated as atomic proportions. The relationship between Th and Ca is shown in fig. 3. The reduced major axis for all analyses in the range 0.20–0.35 Th has been added; the slope of this line is $Ca/Th = 0.96$. The approximate 1:1 atomic relationship between these elements implies that the substitution of Ca^{2+} for REE^{3+} controls the entry of Th^{4+} into monazite: i.e. $Ca^{2+} + Th^{4+} \rightleftharpoons 2REE^{3+}$. A similar plot of Si and Th shows no increase in Si with increasing Th in the range 0.20–0.35 Th.

Therefore, of the two major substitutions described by Gramaccioli and Segalstad, namely $Ca^{2+} \rightleftharpoons REE^{3+}$ and $Si^{4+} \rightleftharpoons P^{5+}$ it appears that

TABLE I. Electron microprobe analyses of monazites from Type I granite. Analysis v is a xenotime analysis reproduced from Amli (1975).

	a	b	c	d	e	f	g	h	i	j	k	l	m	n	o	p	q	r	s	t	u		v
Al_2O_3	0.06	0.03	0.03	0.00	0.18	0.18	0.03	0.06	0.03	0.06	0.32	1.20	0.06	0.06	0.03	0.03	0.06	0.06	0.03	0.06	0.06	SiO_2	0.32
SiO_2	0.38	0.41	0.46	0.52	0.44	0.57	0.46	0.46	0.49	1.48	1.08	2.97	0.44	0.58	0.49	0.44	0.49	0.49	0.49	0.49	0.38	P_2O_5	34.19
P_2O_5	28.95	28.93	28.48	28.58	28.84	28.44	28.70	28.91	29.11	28.55	27.55	25.64	29.21	27.87	28.31	28.25	28.87	28.68	28.55	28.63	28.96	CaO	nd
CaO	1.50	1.60	1.73	1.47	1.73	1.66	1.60	1.65	1.71	1.52	2.61	3.50	1.44	1.11	1.65	1.70	1.59	1.45	1.55	1.57	1.43	Y_2O_3	47.88
Y_2O_3	0.78	1.11	1.07	0.76	1.11	1.17	0.85	0.91	0.89	0.77	1.15	1.08	0.92	0.34	0.94	1.02	0.78	0.75	0.81	1.06	0.67	La_2O_3	nd
La_2O_3	15.27	14.79	14.30	15.64	14.19	14.18	15.84	16.02	15.01	14.94	13.33	12.79	15.73	17.01	14.82	14.60	15.26	15.93	14.66	14.82	15.35	Ce_2O_3	nd
Ce_2O_3	30.32	30.61	27.67	30.63	30.04	30.07	30.49	29.91	29.23	28.04	27.54	25.15	30.00	31.19	31.14	30.39	29.58	30.47	31.07	30.84	31.93	Pr_2O_3	nd
Pr_2O_3	2.52	-	2.55	2.81	2.53	2.82	2.76	2.74	2.80	2.40	2.22	1.85	2.48	2.79	2.50	2.75	2.57	-	2.51	-	-	Nd_2O_3	nd
Nd_2O_3	9.85	10.37	10.30	10.12	10.24	9.54	9.51	9.38	10.18	10.04	9.02	6.55	8.91	10.07	9.65	10.09	10.34	10.31	10.13	10.61	10.39	Sm_2O_3	0.11
Sm_2O_3	1.57	1.52	1.56	1.38	1.53	1.58	1.34	1.37	1.50	1.41	1.41	0.99	1.38	1.18	1.49	1.56	1.50	1.35	1.52	1.57	1.47	Eu_2O_3	nd
Dy_2O_3	0.07	0.13	0.20	0.06	0.08	0.19	0.04	0.09	0.10	0.07	0.20	0.16	0.13	0.03	0.14	0.05	0.05	0.04	0.10	0.16	0.04	Gd_2O_3	1.23
PbO	0.20	0.20	0.21	0.16	0.21	0.20	0.18	0.16	0.16	0.18	0.21	0.26	0.18	0.15	0.20	0.16	0.15	0.16	0.15	0.18	0.15	Tb_2O_3	0.25
ThO_2	7.85	7.59	8.57	8.04	8.91	8.45	8.33	8.45	9.05	7.33	10.89	12.61	7.47	6.42	8.93	8.71	8.27	7.16	8.44	8.07	7.80	Dy_2O_3	3.60
UO_2	-	-	-	0.64	-	0.24	0.58	0.50	0.55	-	-	-	-	0.77	2.28	0.48	0.82	-	-	0.91	0.30	Ho_2O_3	0.84
																						Er_2O_3	3.64
Total	99.20	97.29	97.13	100.81	100.03	99.29	100.71	100.61	100.81	96.82	97.53	94.75	98.38	99.57	102.57	100.23	100.76	96.85	100.01	98.97	98.93	Tm_2O_3	0.58
																						Yb_2O_3	4.41
																						Lu_2O_3	0.58
Al	0.011	0.005	0.005	0.000	0.033	0.033	0.005	0.011	0.005	0.011	0.060	0.226	0.011	0.011	0.005	0.005	0.011	0.011	0.005	0.011	0.011		
Si	0.061	0.065	0.074	0.082	0.069	0.091	0.073	0.072	0.076	0.234	0.171	0.475	0.069	0.093	0.077	0.069	0.077	0.079	0.078	0.078	0.061	Total	97.63
P	3.886	3.916	3.885	3.818	3.847	3.823	3.817	3.827	3.844	3.844	3.722	3.480	3.907	3.800	3.769	3.802	3.843	3.902	3.831	3.782	3.907	Si	0.0109
Ca	0.255	0.274	0.298	0.248	0.292	0.282	0.269	0.276	0.285	0.260	0.446	0.601	0.243	0.192	0.278	0.290	0.268	0.250	0.263	0.268	0.243	P	0.9891
Y	0.066	0.095	0.091	0.064	0.093	0.099	0.071	0.076	0.074	0.065	0.098	0.092	0.078	0.029	0.078	0.086	0.065	0.064	0.068	0.090	0.056	Y	0.8706
La	0.893	0.972	0.850	0.910	0.824	0.831	0.918	0.924	0.863	0.876	0.784	0.756	0.916	1.011	0.860	0.856	0.885	0.944	0.857	0.873	0.902	Sm	0.0013
Ce	1.753	1.792	1.620	1.769	1.733	1.748	1.754	1.712	1.669	1.632	1.609	1.476	1.735	1.839	1.793	1.769	1.703	1.793	1.803	1.803	1.863	Gd	0.0139
Pr	0.146	-	0.150	0.162	0.145	0.163	0.158	0.156	0.159	0.139	0.129	0.108	0.143	0.164	0.143	0.159	0.147	-	0.145	-	0.591	Tb	0.0028
Nd	0.558	0.592	0.593	0.570	0.576	0.541	0.533	0.524	0.567	0.570	0.514	0.375	0.503	0.579	0.542	0.573	0.581	0.592	0.573	0.605	0.081	Dy	0.0397
Sm	0.086	0.083	0.086	0.075	0.083	0.086	0.072	0.074	0.080	0.077	0.077	0.055	0.075	0.065	0.081	0.085	0.081	0.075	0.083	0.086	0.002	Ho	0.0091
Dy	0.003	0.007	0.011	0.003	0.004	0.009	0.002	0.004	0.005	0.004	0.010	0.008	0.007	0.001	0.007	0.003	0.003	0.002	0.005	0.008	0.006	Er	0.0391
Pb	0.008	0.008	0.009	0.006	0.008	0.008	0.007	0.006	0.006	0.007	0.008	0.010	0.007	0.006	0.008	0.006	0.006	0.006	0.006	0.007	0.008	Tm	0.0061
Th	0.283	0.276	0.314	0.288	0.320	0.305	0.298	0.300	0.321	0.265	0.395	0.460	0.269	0.235	0.320	0.315	0.296	0.262	0.305	0.293	0.283	Yb	0.0459
U	-	-	-	0.021	-	0.008	0.019	0.016	0.018	-	-	-	-	0.026	0.075	0.026	0.027	-	-	0.030	0.010	Lu	0.0060
Total	8.009	7.985	7.986	8.016	8.027	8.019	7.996	7.978	7.972	7.984	8.023	8.122	7.963	8.051	8.036	8.044	7.993	7.980	8.022	8.024	8.016		2.0345

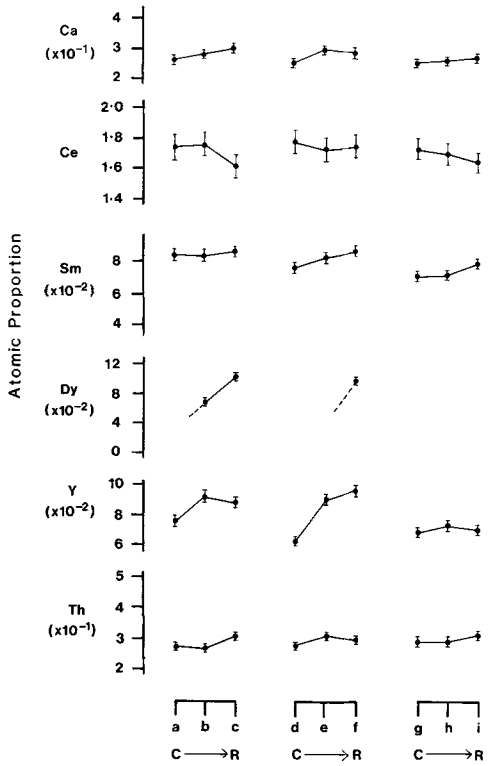

FIG. 2. Three electron microprobe traverses of monazites from Type I granite (analyses *a–i*, Table II). Traverses are from core to rim: error bars are 5%.

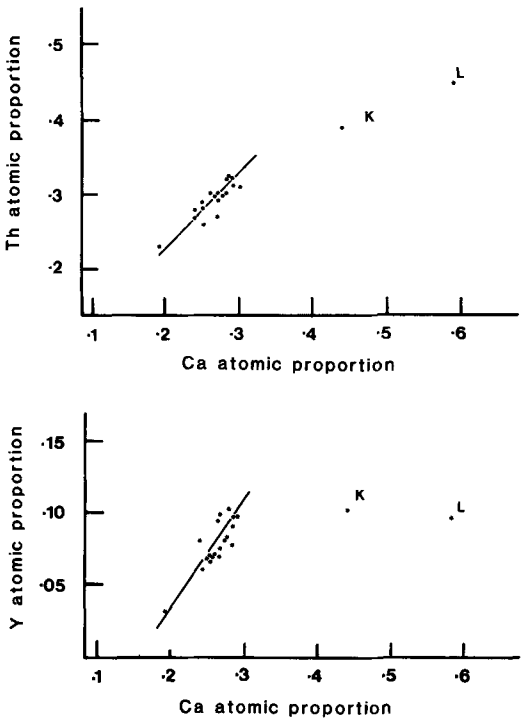

FIGS. 3 and 4. FIG. 3 (*top*). The ionic relationship between Th and Ca within monazites from Type I granite. FIG. 4. The ionic relationship between Y and Ca within monazites from Type I granite. Analyses *K* and *L* are of hydrothermally altered crystals.

the former is responsible for the incorporation of Th into the monazites of the Carnmenellis pluton. This substitution has been previously recognized in monazites of both metamorphic (Bowie and Horne, 1953; Mohr, 1984) and pegmatitic (Gramaccioli and Segalstad, 1978) origin.

Mohr (1984), in an electron microprobe study of zoned monazite porphyroblasts in pelitic schists from N. Carolina suggested that an increase in Th and Ca in monazite might correlate with zonation of the *REE* and Y. This trend is explained by a decrease in ionic size with increasing atomic number of the *REE* and a slight decrease of unit cell dimensions of monazite due to an increased content of Th and Ca. Y^{3+}, with an ionic radius 0.06 Å lower than Dy^{3+} would be expected to show the greatest relative enrichment due to an increase in Th and Ca. The variation of Y and Ca in the monazites of the Carnmenellis granite is shown in fig. 4. The high linear correlation coefficient ($r = +0.84$) suggests that Ca (and hence Th) enriched monazites are also relatively enriched in the Y group *REE*.

From figs. 3 and 4 it is apparent that two of the monazite analyses (labelled K and L) are anomalous as they plot away from the reduced major axes. These analyses are from the outer zone of a monazite, showing marginal dissolution, included within a partially chloritized biotite. There is a decrease in P insufficiently balanced by increasing Si, and increases in Ca and Th with a corresponding decrease in the *LREE* (Table 1). It is suggested that the enrichment in Ca, Th, and Si is the result of hydrothermal alteration, and this will be discussed in a further section.

Inductively Coupled Plasma Spectrometry analyses

It is very difficult to analyse for Gd, Ho, Eu, or Er using electron probe microanalysis because of peak interferences (N. Charnley, pers. comm.) and therefore Inductively Coupled Plasma Source Spectrometry has been used to obtain *REE* patterns of monazites and zircons separated from Types I and II granite. The procedure for this technique has been described by Walsh *et al.* (1981) who referred to the problem of incomplete dissolution of certain

TABLE II.

ICP Spectrometry data for granite types within the Carnmenellis pluton and for mineral separates from Type I granite. Values given as ppm for whole rock analyses and zircon separate and as wt % oxide for monazites.

	(ppm)									(wt % oxide)		
	1	2	3	4	5	6	7	8	9	10	11	12
La	38.12	33.42	29.75	19.13	6.65	26.03	30.35	34.08	1674	10.46	11.45	10.62
Ce	77.83	68.54	60.61	37.79	12.96	52.47	62.42	69.53	3662	25.46	28.31	23.91
Pr	8.57	7.53	6.89	4.24	1.38	5.83	6.95	7.72	448	1.34	1.39	1.63
Nd	34.48	30.06	27.82	17.55	5.88	23.70	28.18	30.91	1559	8.96	9.48	9.17
Sm	6.45	5.83	5.19	3.57	1.32	4.42	5.35	5.85	295	1.52	1.74	1.57
Eu	0.69	0.79	0.64	0.65	0.10	0.64	0.66	0.68	6	0.02	0.03	0.02
Gd	4.41	4.03	3.52	2.68	1.00	3.07	3.69	4.04	221	0.84	0.99	0.89
Dy	2.79	2.57	2.29	1.91	1.09	2.09	2.38	2.55	228	0.29	0.36	0.32
Ho	0.46	0.43	0.37	0.29	0.19	0.33	0.39	0.45	62	0.04	0.05	0.05
Er	1.36	1.23	1.13	0.90	0.67	1.05	1.18	1.25	265	0.10	0.13	0.11
Yb	1.04	0.93	0.86	0.71	0.72	0.85	0.92	0.98	481	0.02	0.05	0.03
Lu	0.14	0.13	0.12	0.09	0.09	0.10	0.12	0.13	96	0.00	0.01	0.00

Type I (1, 3): Type II (2): Type III (4): Tourmaline microgranite (5): Chloritised Type I (6, 7, 8). Zircon Type I (9): Monazite Type I (10, 12): Monazite Type II (11).

resistant minerals such as zircon. To minimize the possibility of incomplete dissolution of the mineral separates in this study, the samples were diluted in the rock powder of a harzburgite, the *REE* pattern of which had previously been determined using Isotope Dilution Mass Spectrometry. The harzburgite possesses a flat *REE* pattern ($La_N = 1.9$; $Lu_N = 2.0$) with a slight negative Eu anomaly (M. Crewe, pers. comm.). This 'background' *REE* content was subtracted from the resulting analyses, which were then multiplied by the dilution factor to obtain the *REE* pattern. Whole-rock *REE* analyses of Types I and II granite were made for comparison with the monazite and zircon patterns, as well as a sample of Type III granite, a tourmaline microgranite sheet, and three chloritized granites. The ICP analyses are given in Table II; figs. 5, 6, 7, and 9 have been constructed using the chrondrite normalizing values of Nakamura (1974).

Whole-rock REE *patterns.* The biotite granites have *LREE* enriched patterns with slight negative Eu anomalies (fig. 5). There is a depletion in *REE* from Types I and II granite to Type III granite. However, Eu is not depleted in this differentiation series, remaining at a level of between 8–10 Eu_N. This results in a decrease in the negative Eu anomaly (which is conventionally expressed as Eu/Eu*) from 0.48 to 0.62. The tourmaline microgranite sheet, which cuts Type I granite, has a lower *LREE* enrichment and possesses a strong negative Eu anomaly.

Monazite REE *patterns.* Monazites from three

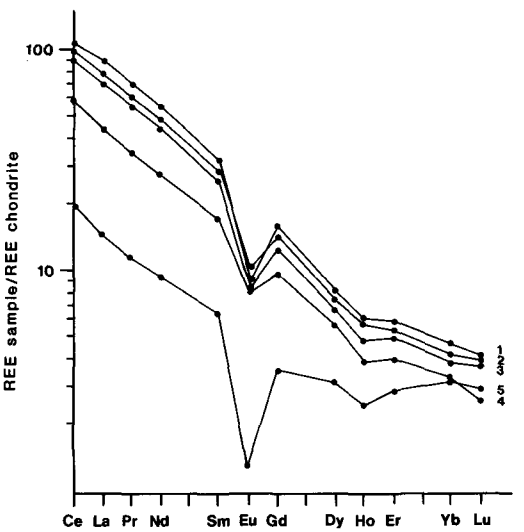

FIG. 5. *REE* patterns of granite types within the Carnmenellis pluton. Type I granite (analyses 1 and 3), Type II (analysis 2), Type III (analysis 4), tourmaline microgranite (analysis 5).

granite samples were investigated; two from Type I granite and one from Type II granite. Samples 10 and 11 were diluted 200 times and shows a minor negative Pr anomaly, whereas sample 12, which was diluted 400 times shows no such feature. The Pr 'anomaly' is possibly due to some feature of the sample preparation procedure. Nevertheless, there are several points of interest in the monazite patterns (fig. 6). The *LREE* 'slope' of the monazite is identical to the *LREE* 'slope' of the whole rock; the negative Eu anomaly is greater than the whole rock anomaly by a factor of 8, and the depletion in *HREE* is greater than the whole-rock values by a factor of at least 6. The divergence of the three patterns in the *HREE* is considered to be due to slight contamination of the monazite sample by *HREE*-rich minerals such as xenotime or zircon.

The strong negative Eu anomaly results from the exclusion of Eu^{2+} from the REE^{3+} site within the monazite structure.

Zircon REE *pattern.* A zircon separate from Type I granite was diluted 40 times and analysed for *REE* (analysis 9, Table I). The *REE* pattern is given in fig. 7 and displays a U shape, with the minimum at Dy, and a negative Eu anomaly. The mineral/matrix distribution coefficients are calculated, and show a constant K_D of approximately 45 for the elements La–Gd, a K_D of 8 for Eu, and a sharp increase in K_D from 82–669 for the elements Dy–Lu. The K_D values obtained for the *LREE* are a factor of 20 higher than those given by Nagasawa (1970) whilst the K_D values for the elements Dy–Lu exceed the values of Nagasawa by a factor of only 2. It seems likely, therefore, that the zircon separate used in this study is contaminated with a *LREE*-rich heavy mineral, presumably monazite. It can be calculated that the contamination amounts to approximately 1% monazite; removal of this contamination produces a *HREE* enriched pattern with a less pronounced negative Eu anomaly (Eu/Eu* = 0.15).

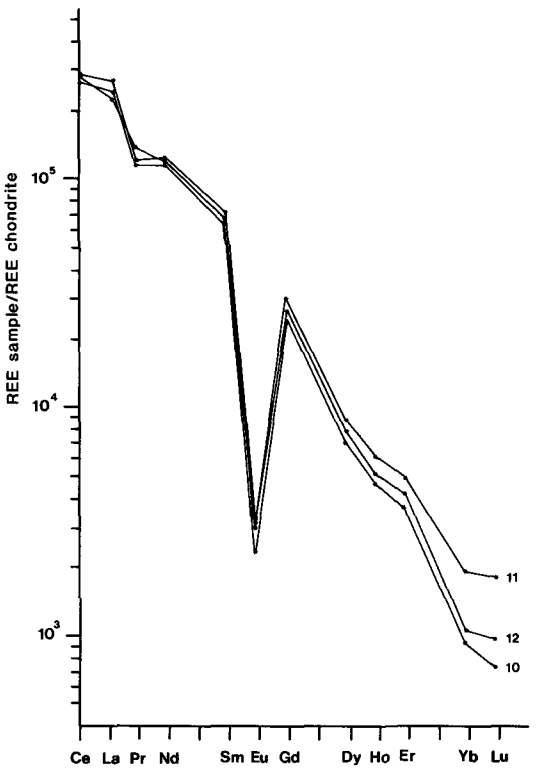

FIG. 6. *REE* patterns of monazites from the Carnmenellis pluton. Type I granite (analyses 10 and 12), Type II granite (analysis 11).

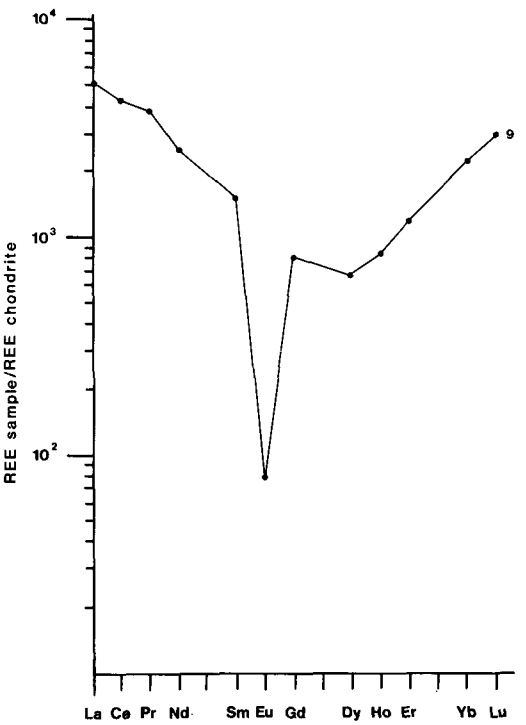

FIG. 7. *REE* pattern of a zircon (analysis 9) from Type I granite. The mineral separate is thought to be contaminated with monazite, which explains the *LREE* enrichment.

The zircon *REE* pattern given in fig. 7 may be used, however, to provide a maximum concentration of *REE* within the zircons of Type I granite, since contamination by monazite and xenotime

will increase the values of the *LREE* and *HREE*, respectively, within the mineral separate.

The partitioning of REE *between the minerals of the Carnmenellis granite*

In order to model quantitatively the distribution of *REE* in the Carnmenellis pluton, some assumptions must be made about the abundance of the accessory minerals monazite, apatite, xenotime, and zircon. XRF data from the biotite granites is presented in Jefferies (1984) for the trace element pairs Zr–Th and Ce–Th and the equation of the reduced major axis (RMA) for Ce–Th is calculated as Ce(ppm) = 4.3 Th(ppm) + 9.3. The mean Ce_2O_3 content of the monazites in Table I is 30.2% and the mean ThO_2 content is 8.1% (excluding analyses *k* and *l* which are hydrothermally altered). The mean Ce/Th ratio given by the electron microprobe data is therefore 3.6, and the similarity between this value and the Ce/Th ratio of 4.3 from the whole-rock XRF analyses suggests that most, if not all, Ce in the granites is contained in monazite.

It is realistic to attribute all Zr in peraluminous granites to zircon, which allows the weight percentage of zircon in the Carnmenellis granite to be calculated. The abundance of apatite is calculated by allotting all P_2O_5, after that allocated to monazite, to apatite. Finally, the abundance of xenotime is estimated from the accessory mineral study (Jefferies, 1984) in which it was shown that xenotime is fifty times rarer than monazite.

Mineral/melt distribution coefficients in rhyolitic rocks have been published for the minerals zircon, apatite, potassium feldspar, and plagioclase feldspar (Nagasawa, 1970; Schnetzler and Philpotts, 1970), and the *REE* content of monazites from the Carnmenellis granite is presented in an earlier section of this paper. The zircon *REE* data of Nagasawa is preferred to those obtained from the zircons of Type I granite, because of the contamination problems in the latter. The K_D values of Nagasawa (1970) have therefore been used in estimating the zircon contribution to the whole-rock *REE* pattern, plotted in fig. 8.

Fig. 8 is constructed such that the sum of the percentage whole-rock Ce contributions of the individual minerals is equal to the whole-rock Ce content, and hence sums to 100%. The only unknown in this calculation is the abundance of monazite, since it obviously cannot be assumed that all Ce is contained in this mineral. But, by taking $Ce_{\text{sum of minerals}} = Ce_{\text{whole rock}}$, the monazite abundance can be calculated.

By combining the modal data from Type I Carnmenellis granite (Al Turki and Stone, 1978) with the K_D values calculated by the above authors, the feldspars emerge as the principal Eu-bearing minerals—plagioclase contributing 4.4 Eu_N and potassium feldspar 3.4 Eu_N towards the whole-rock total of 9.8 Eu_N.

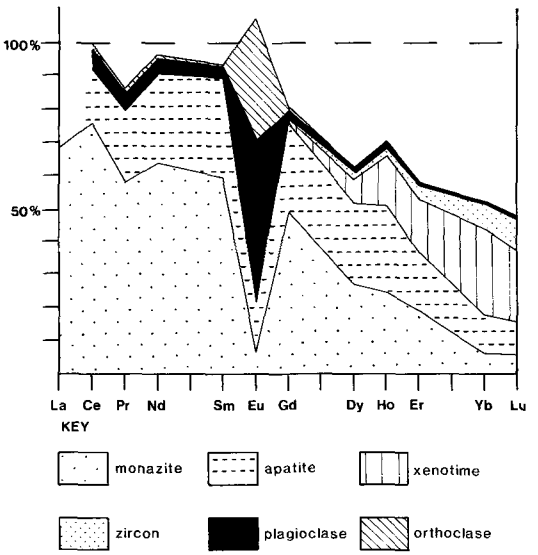

FIG. 8. Cumulative *REE* contents of the minerals within Type I granite, expressed as a percentage of the whole-rock abundance.

Zircon is often invoked as a major source of *HREE* in granitic rocks (Watson, 1979; Hanson, 1978). However, the mean Zr content of Types I and II granite is only 110 ppm (Jefferies, 1984), low in comparison with the 'average' granite Zr content of 175 ppm (Turekian, 1977). Less than 10% of the *HREE* content of the granite is partitioned into zircon if the K_D values determined by Nagasawa (1970) are used. A maximum possible figure of 20% is obtained if the K_D values calculated from analysis 9 (Table I) are used instead. It is apparent, therefore, that zircon does not contribute significantly to the *HREE* content of the Carnmenellis granite.

No *REE* data have been obtained from xenotimes within the Carnmenellis granite, and few chemical analyses of this mineral have been published from other granitic rocks. Amli (1975) presented electron microprobe analyses of xenotime from a granitic pegmatite and his analysis 15 (reproduced in Table I) is assumed to be an approximation of the xenotime chemistry from Carnmenellis. Using this data it is possible to estimate the contribution of xenotime to the whole-rock *REE* total. From fig. 8 it is

apparent that xenotime is more important than zircon as a *HREE* source. The contribution of xenotime to the whole-rock *REE* budget is, however, a crude approximation as a result of the method used to calculate the mineral abundance and the assumption that the chemistry is identical to the pegmatitic xenotime of Amli (1975).

The distribution of the *REE* between the various minerals of Type I Carnmenellis granite are plotted in fig. 8. It is evident that the radioactive accessory mineral assemblage (monazite–xenotime–apatite–zircon) concentrates most of the trivalent *REE*, whilst the feldspars contain approximately 80% of the Eu. Monazite is the most important *REE*-bearing accessory mineral, containing approximately 75% of the *LREE*, whilst xenotime, apatite, zircon, and monazite partition the *HREE* between them.

The Lu value calculated on the contribution of individual minerals is only half that of the whole rock Lu value. This is considered to be due to an underestimation in the abundance of xenotime, since the concentration of the other *HREE*-bearing phases are estimated with greater accuracy.

The interpretation of variations in the REE *during differentiation of the Carnmenellis granite*

Having established the sites for the *REE* within the biotite granites, it is possible to interpret the variations in the whole-rock patterns with more confidence. The decreasing concentration of all *REE* except Eu during granite differentiation is due to lower concentrations of accessory minerals, as is suggested by the lower levels of Th and Zr in the later emplaced biotite granites (Jefferies, 1984).

The modal proportions of plagioclase in Types I and III granite are identical (Al Turki and Stone, 1978) and the shallowing Eu anomaly is solely due to the depletion of Sm and Gd, whilst Eu (which is preferentially excluded from monazite because of its divalent state) remains at a constant level.

The low levels of *REE* within the tourmaline microgranites is in agreement with a late differentiate origin for these sheets. However, continued fractionation of the accessory minerals alone cannot produce the observed *REE* pattern of the microgranite sheet (sample 5), as a pronounced negative Eu anomaly is still present. The composition of the plagioclase within the tourmaline microgranite sheets is albitic, and since it has been demonstrated by Schnetzler and Philpotts (1970) that the uptake of Eu^{2+} by this mineral depends upon the anorthite content (since Eu^{2+} substitutes for Ca^{2+} in the plagioclase structure) this will reduce the Eu content of the plagioclase. In turn this will reduce the Eu content of the microgranite and promote the formation of a negative Eu anomaly.

Hydrothermal alteration of monazite

Alderton *et al.* (1980) investigated the mobilization of the *REE* in some hydrothermally altered Cornish granites, and demonstrated that the *REE* may be mobilised during certain hydrothermal alteration events. Only the process of chloritization was considered in this paper, as chloritization of biotite has taken place, in varying intensities over much of the Carnmenellis pluton. Chloritization may therefore have had an effect on the granite *REE* analyses presented in Table I. The process of chloritization, in which biotite is replaced by chlorite (variety ripidolite) and plagioclase is moderately sericitized, was described by Alderton *et al.* (1980) as one of weak hydrogen metasomatism, since the whole-rock geochemistry remained unaffected. It must not be confused with vein-related chloritization which results in Fe enrichment and the formation of a quartz–chlorite ± muscovite assemblage.

The *REE* patterns of three chloritized Type I granites from Holman Test Mine, in the northern part of the Carnmenellis pluton (GR SW 657 366), are plotted in fig. 9. A comparison of this figure with the *REE* patterns of 'fresh' granites (fig. 5) demonstrates that the *REE* are immobile, on the scale of a hand sample, during this hydrogen metasomatism process.

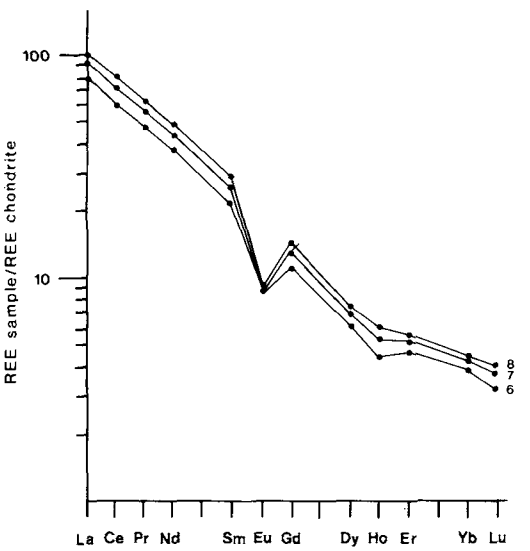

FIG. 9. *REE* patterns of chloritized granite from the northern part of the Carnmenellis pluton.

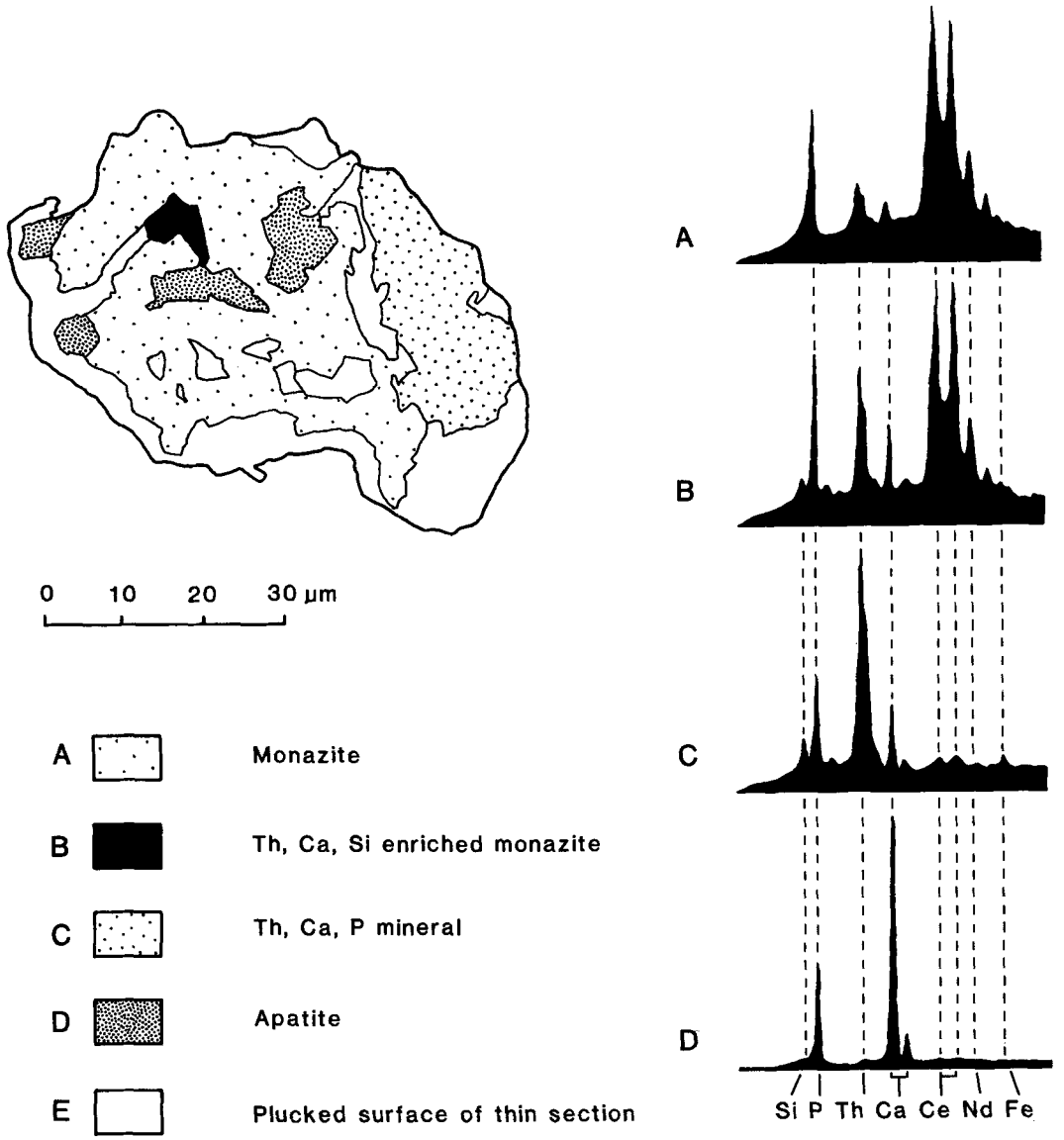

FIG. 10. A sketch of a hydrothermally altered monazite crystal in a chloritized granite. Energy dispersive X-ray spectra demonstrate the chemical changes taking place during alteration.

However, monazites within chloritized granites are commonly corroded and show extensive replacement by alteration products. A sketch of a corroded monazite, made from an SEM image, is given in fig. 10. Qualitative energy dispersive X-ray spectra of various points within the crystal, produced using a Link microanalyser, are added. The monazite shows replacement by apatite (Ca, P) and Ca, Th and Si-rich minerals. *REE* have been mobilized from the monazite, but from fig. 9, they are not depleted from the granite on a larger scale.

The most probable site for the *REE*, released during the breakdown of monazite, is fluorite. This mineral is a ubiquitous product of this style of chloritization, being precipitated at the sites of liberation of F during alteration of the biotite (Durrance *et al.*, 1982).

It seems probable, therefore, on the basis of the

alteration style of monazite in chloritized granite that the increase in Ca, Th, and Si in microprobe analyses *k* and *l* is the result of hydrothermal alteration.

Conclusions

The *REE* within the biotite granites of the Carnmenellis pluton are strongly partitioned into the radioactive accessory mineral assemblage, which consists of monazite–xenotime–zircon–apatite and uraninite. Only Eu, presumably existing as a divalent ion, substitutes in significant amounts into the essential minerals, in this case the feldspars.

Unless the partitioning of *REE* into accessory minerals is recognized, variations in the *REE* patterns during granite differentiation may be misinterpreted. For example, the decreasing negative Eu anomaly during differentiation of the biotite granites may be explained in terms of plagioclase fractionation if the importance of monazite was overlooked.

The concentration of *REE* within the accessory minerals of granitic rocks limits the petrogenetic significance which may be attached to these elements, since the behaviour of the accessory minerals during magmatic differentiation is less well understood than that of the essential minerals.

Finally, it is possible that granitic accessory minerals, such as zircon, monazite, and xenotime, may have a restite origin as was suggested for some zircons from the Caledonian granites of Scotland (Pidgeon and Aftalion, 1978). This will further complicate any petrogenetic modelling attempted on the partial melting of a source region to produce a granitic magma since *REE*-bearing minerals may be incorporated into the granitic magma without having undergone melting.

Acknowledgements. I wish to thank Dr Norman Charnley, University of Oxford, for carrying out the electron microprobe analyses. I also thank Simon Chenery and Dr Nick Walsh of Kings College London for sample preparation and ICP Spectrometry data. Dr E. M. Durrance kindly read, and suggested improvements to, an earlier draft of this paper. Financial support for this study was provided by the NERC and CEGB.

REFERENCES

Alderton, D. H. M., Pearce, J. A., and Potts, P. J. (1980) *Earth Planet. Sci. Lett.* **49,** 149–65.

Al Turki, K., and Stone, M. (1978) *Proc. Ussher Soc.* **4,** 182–9.

Amli, R. (1975) *Am. Mineral.* **60,** 607–20.

Basham, I. R., Ball, T. K., Beddoe-Stephens, B., and McMichie, U. (1982) Uranium-bearing accessory minerals and granite fertility: II. Studies of granites from the British Isles. In *Symposium on Uranium Exploration Methods*: Paris 1982 IAEA Vienna.

Bowie, S. H. U., and Horne, J. E. T. (1953) *Mineral. Mag.* **30,** 93–9.

Chayes, F. (1955) *Geol. Mag.* **92,** 364–6.

Compton, P. (1978) *Contrib. Mineral. Petrol.* **66,** 283–93.

Deer, W. A., Howie, R. A., and Zussman, J. (1962) *Rock Forming Minerals*, **5,** 342–3. Longmans, London.

Durrance, E. M., Bromley, A. V., Bristow, C. M., Heath, M. J., and Penman, J. M. (1982) *Proc. Ussher Soc.* **5,** 304–20.

Fourcade, S., and Allegre, C. J. (1981) *Contrib. Mineral. Petrol.* **76,** 177–95.

Ghosh, P. K. (1934) *Q.J. Geol. Soc.* **90,** 240–76.

Gramaccioli, C. M., and Segalstad, T. V. (1978) *Am. Mineral.* **63,** 757–61.

Hanson, G. N. (1978) *Earth Planet. Sci. Lett.* **38,** 26–43.

Jefferies, N. L. (1984) *Proc. Ussher Soc.* **5,** 35–41.

Le, V. T., and Stussi, J. M. (1973) *Sci. Terre*, **18,** 353–79.

McCarthy, T. S., and Kable, E. J. D. (1978) *Chem. Geol.* **22,** 21–9.

Mohr, D. W. (1984) *Am. Mineral.* **69,** 98–103.

Nagasawa, H. (1970) *Earth Planet. Sci. Lett.* **9,** 359–64.

Nakamura, N. (1974) *Geochim. Cosmochim. Acta*, **38,** 757–75.

Pagel, M. (1982) *Mineral. Mag.* **46,** 149–61.

Pidgeon, R. T., and Aftalion, M. (1978) In *Crustal Evolution in Northwestern Britain and adjacent regions* (D. R. Bowes and B. E. Leake, eds.). Geol. J. Spec. Iss. No. 10, 183–220.

Schnetzler, C. C., and Philpotts, J. A. (1970) *Geochim. Cosmochim. Acta*, **34,** 331–40.

Stone, M. (1979) *Proc. Ussher Soc.* **4,** 370–9.

Turekian, K. K. (1977) In *Encyclopedia of Science and Technology*. 4th edn. McGraw-Hill, New York, 627–30.

Walsh, J. N., Buckley, F., and Barker, J. (1981) *Chem. Geol.* **33,** 141–53.

Watson, E. B. (1979) *Contrib. Mineral. Petrol.* **70,** 407–19.

[*Manuscript received 2 May 1984; revised 27 October 1984*]